Fatigue crack initiation and growth on a steel in the very high cycle regime with sea water corrosion

Thierry Palin-Luc [a,*], Rubén Pérez-Mora [a,b], Claude Bathias [c], Gonzalo Domínguez [d], Paul C. Paris [a], Jose Luis Arana [e]

[a] Arts et Métiers ParisTech, Université Bordeaux 1, LAMEFIP, Esplanade des Arts et Métiers, F-33405 Talence Cedex, France
[b] Advanced Technology Center of Queretaro (CIATEQ), Santiago de Queretaro, Mexico
[c] Université Paris X, LEME, 50 rue de Sevres, F-92410 Ville d'Avray, France
[d] University of Michoacan (UMSNH), Santiago Tapia 403, 58000 Morelia, Mexico
[e] University of the Basque Country, ETSI, c/Alameda de Urquijo s/n, 48013 Bilbao, Spain

Keywords:
Gigacycle fatigue
Steel
Sea water corrosion
Crack initiation
Crack growth

This paper is devoted to the effect of corrosion on the gigacycle fatigue strength of a martensitic–bainitic hot rolled steel used for manufacturing offshore mooring chains for petroleum platforms. Smooth specimens were tested under fully reversed tension between 10^6 and 10^{10} cycles in three testing conditions and environments: (i) in air, (ii) in air after pre-corrosion and (iii) in air under real time artificial sea water flow. The fatigue strength at greater than 10^8 cycles is reduced by a factor more than five compared with non-corroded specimens. Fatigue cracks initiate at corrosion pits due to pre-corrosion, if any, or pits resulting from corrosion in real time during the cyclic loading. It is shown that under sea water flow, the fatigue life in the gigacycle regime is mainly governed by the corrosion process. Furthermore, the calculation of the mode I stress intensity factor at hemispherical surface defects (pits) combined with the Paris–Hertzberg–Mc Clintock crack growth rate model shows that fatigue crack initiation regime represents most of the fatigue life.

1. Introduction

Mooring chains for offshore petroleum platforms, designed for 30 years, are loaded in fatigue in sea water environment in the gigacycle regime (around 10^9 cycles). The aim of this study is to investigate the gigacycle fatigue strength of low-alloy steel and the effects on this strength of pre-corrosion and corrosion in sea water environment. Many studies carried out on steel and aluminum alloys in the gigacycle regime have demonstrated that there is not a fatigue limit in such metals after 10^7 cycles as was believed in the past [1,2]. It has been shown that fatigue cracks initiate mainly at surface defects in the short fatigue life range, but may shift to subsurface in the long life range [3]. Other studies have shown that defects like non-metallic inclusions, pores and shrinkages [4] or pits [5–7] are the key factors, which control the fatigue properties of metals in very high cycle fatigue (VHCF). Furthermore, in some works it has been proven that crack initiation dominates the total fatigue life of specimens in gigacycle fatigue [8]. In this study the effect of corrosion on the fatigue strength will be quantified and the assessment of the crack propagation period will allow us to investigate the relationship between crack initiation and crack propagation.

* Corresponding author. Tel.: +33 556 845 360; fax: +33 556 845 366.
E-mail address: thierry.palin-luc@ensam.eu (T. Palin-Luc).

doi:10.1016/j.engfracmech.2010.02.015

Nomenclature

a	crack length
a_{int}	crack length at initiation
a_0	at the corner of the crack growth curve
b	Burger vector
E	Young modulus
N_{Prop}	number of cycles of the crack propagation period
N_{a_i-a}	number of cycles of the long crack growth period
$N_{a_0-a_i}$	number of cycles of the small crack growth period
$N_{a_{\text{int}}-a_0}$	number of cycles of the short crack growth period
R	radius of the hemispherical surface defect
U_o	amplitude of the displacement at the extremities of the specimen
w	specimen width
v	Poisson ratio
ΔK	stress intensity range (mode I)
σ_a	stress amplitude

2. Material and experimental conditions

2.1. Material

The investigated material is a non-standard hot rolled low-alloy steel grade, named R5 according to the international denomination of the International Classification Societies of offshore systems. This steel is usually used to manufacture mooring chains and accessories intended for position mooring applications such as: mooring of mobile offshore units, mooring of floating production units and mooring of offshore loading systems.

This material has a typical fine grain microstructure, composed of tempered martensite and bainite, as shown in Fig. 1a. Its chemical composition is presented in Table 1. This steel is used after a double quenching in water at 920 °C then 880 °C and tempering at 650 °C with water cooling. After this heat treatment its mechanical properties under quasi-static monotonic tension are as follows: hardness 317 HB, yield strength 970 MPa, UTS = 1018 MPa, Young modulus E = 211 GPa. The R5 steel is vacuum degassed with low hydrogen content (1 ppm maximum in the liquid steel after the vacuum treatment) and very low non-metallic inclusions content (Fig. 1b). Typical non-metallic inclusions according to both the ASTM E45 and AMS 2301 standards are indicated in Table 2.

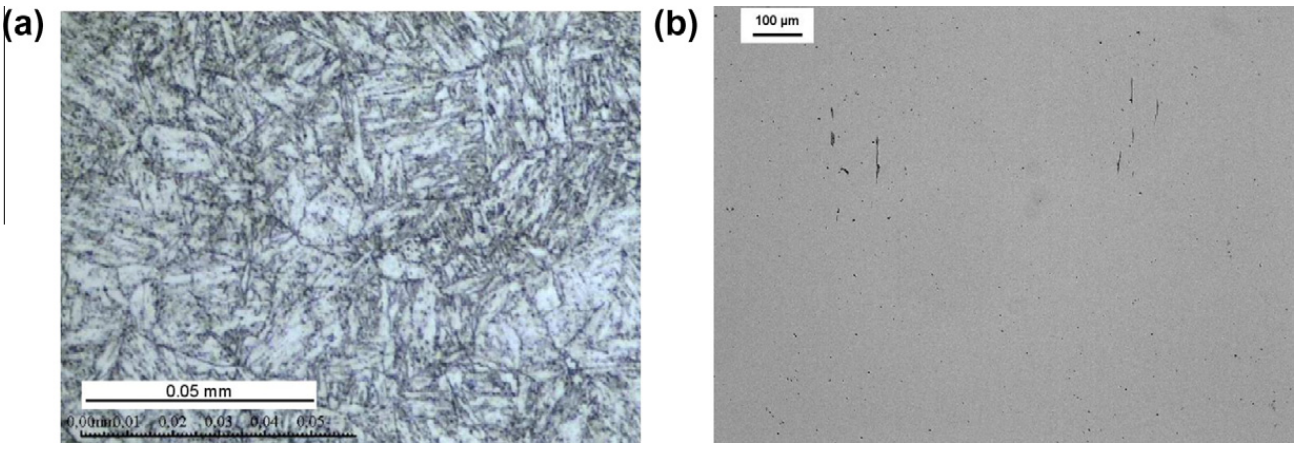

Fig. 1. (a) R5 steel microstructure after nital etching and (b) non-metallic inclusions (in dark).

Table 1
Chemical composition of R5 steel (wt.%, Fe balance).

C	Mn	Si	P	S	Cr	Ni	Mo	V	Cu	O
0.23	1.22	0.3	0.009	0.003	1.07	1.07	0.5	0.09	0.14	12 ppm

Table 2
Non-metallic inclusions content of R5 steel according to ASTM E45 and AMS 2301 standards.

Type A sulphides		Type B alumina		Type C silicates		Type C globular oxides	
Thin	Heavy	Thin	Heavy	Thin	Heavy	Thin	Heavy
0.5	0	1.0	0	0	0	0	0.5

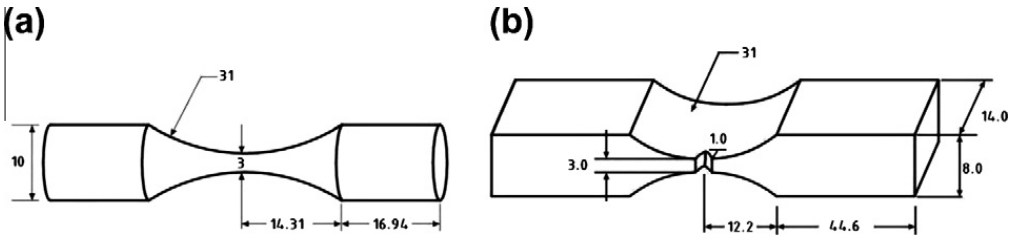

Fig. 2. Specimen geometry for: (a) VHCF tests, $K_t = 1.02$ and (b) crack growth tests (dimensions in mm).

2.2. Fatigue test conditions and geometry of the specimens

2.2.1. Testing machine and geometry of the specimens

Two types of fatigue tests have been carried out: crack initiation and crack growth. All were carried out at 20 kHz with an ultrasonic fatigue testing machine [1] under fully reversed tension ($R = -1$) (details can be found in [1]). Since the amplifier and the specimen must work at resonance, the specimen geometry was designed using the elastic wave theory. Fig. 2 shows the dimensions of the two types of specimens: (i) for VHCF tests (crack initiation) and (ii) fatigue crack growth (FCG) tests. The geometry of these last specimens (FCG) was designed according to the work of Wu and Sun [9,10]. The crack growth was measured with an optical binocular microscope with a maximum magnification 200×. The roughness of the tested area of the VHCF specimens was $Ra = 0.6$ μm. The VHCF specimens were tested under three different conditions: (i) without any corrosion (virgin state), (ii) after pre-corrosion and (iii) under real time artificial sea water flow. All the VHCF tests were calibrated by using a wide band (100 kHz) strain gauge conditioner and a longitudinal strain gauge glued on the specimen surface. Such calibration allow the authors to be sure of the local strain amplitude and mean value in the smallest cross section of the specimen. These tests were carried out until a decrease of the resonance frequency of 0.5 kHz due to the presence of a crack; some times the specimen was broken in two parts but not always; this is discussed at the end of this paper together with the duration of crack growth period compared to the total life.

2.2.2. Corrosion of the specimens

The pre-corrosion of the specimens (before any mechanical loading) was carried out according to the ASTM G85 standard. The specimens stayed 600 h in a salt fog corrosion chamber under temperature and humidity control with the following conditions: 35 °C with 95% of humidity. The salt solution contains 5% of NaCl, its pH is 6.6 and it is applied in the chamber with a rate flow of 1.52 ml/h. After the pre-corrosion process the specimens were removed from the corrosion chamber, first chemically cleaned and then cleaned with emery paper to remove the oxide layer. Many corrosion pits were created by the salt fog, their diameter were between 30 and 80 μm (Fig. 3).

To carry out the VHCF crack initiation tests in sea water environment a special corrosion cell was home designed and made (Fig. 4). To avoid any cavitation and to be representative of the splash zone on the mooring chain (interface between the ocean and the atmosphere), it was decided to test the specimens under sea water flow without any immersion. The experimental setup is based on a peristaltic pump which creates a flow of artificial sea water (100 ml/min) on two opposite sides of the specimen surface in the tested area (diameter 3 mm). The sea water used was the A3 standard synthetic sea water; its chemical composition is (wt.%): 24.53% NaCl, 5.2% MgCl, 4.09% Na_2SO_4, 1.16% Ca_2Cl, 0.695% CaCl and 0.201% $NaHCO_3$. The pH of this solution is 6.6 and no electrical potential was applied between the corrosion solution and the specimen.

2.2.3. Fatigue crack growth tests

Fatigue crack growth tests were carried out under fully reversed loading ($R = -1$), following a similar methodology as described in the ASTM E647 standard. But because with an ultrasonic fatigue testing device the specimen is loaded under displacement control, the range of the stress intensity factor, ΔK, was computed according to the equation proposed in Refs. [9,10]:

$$\Delta K = U_0 \left(\frac{E}{1 - \nu^2} \right) \sqrt{\frac{\pi}{a}} Y(a/w) \tag{1}$$

where U_0 is the amplitude of the displacement imposed at the top of the specimen by the horn, E is the Young modulus and ν the Poisson ratio of the material, $Y(a/w)$ is a function depending on the specimen geometry, a is the crack length and w the width of the specimen:

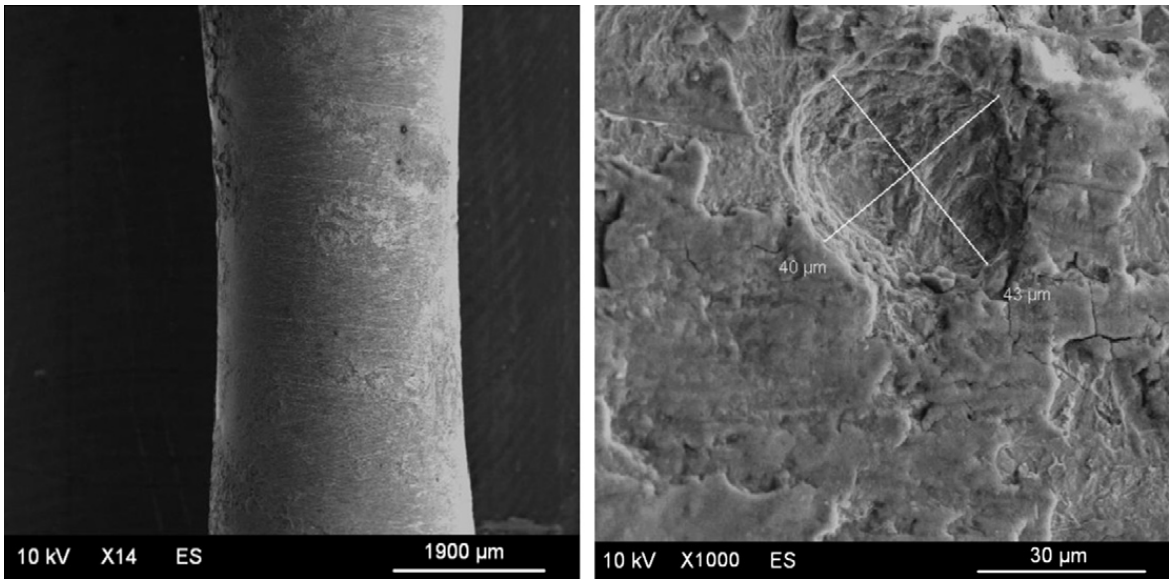

Fig. 3. Typical corrosion pits at the surface of pre-corroded specimen (before any cyclic loading).

Fig. 4. Corrosion cell with peristaltic pump in order to circulate A3 sea water.

$$Y(a/w) = 0.635(a/w) + 1.731(a/w)^2 - 3.979(a/w)^3 + 1.963(a/w)^4$$

3. Results and discussion

3.1. Fatigue crack initiation tests

Fig. 5 shows the S–N curves of the crack initiation tests. This figure shows a decreasing (around 50 MPa) of the fatigue strength for the specimens with pre-corrosion compared to the specimens without corrosion. Furthermore, the scatter of the fatigue strength of pre-corroded specimens is larger than for virgin ones. The effect of sea water flow during VHCF fatigue tests is very important. Indeed, for the specimens tested under sea water flow, the fatigue strength at 10^7 cycles is around 300 MPa, not far from the value for pre-corroded specimens (360 MPa), whereas at 3×10^8 cycles the fatigue strength is around 100 MPa only. At this fatigue life the fatigue strength decreasing was −71% compared to pre-corroded specimens and −74% compared to virgin specimens. The fatigue strength decreased significantly in the tests under real time artificial sea water flow due to the detrimental corrosive effect.

3.2. Fractography analysis

Except for some unusual internal crack initiation (Fig. 6), fatigue cracks initiated mainly at the specimen surface over the cycle range (10^6–10^9 cycles). Surface defects were the origin of the cracks for non-corroded specimens and corrosion pits for pre-corroded specimens (Fig. 7) and specimens tested under sea water flow (Fig. 8). For the specimens tested under sea

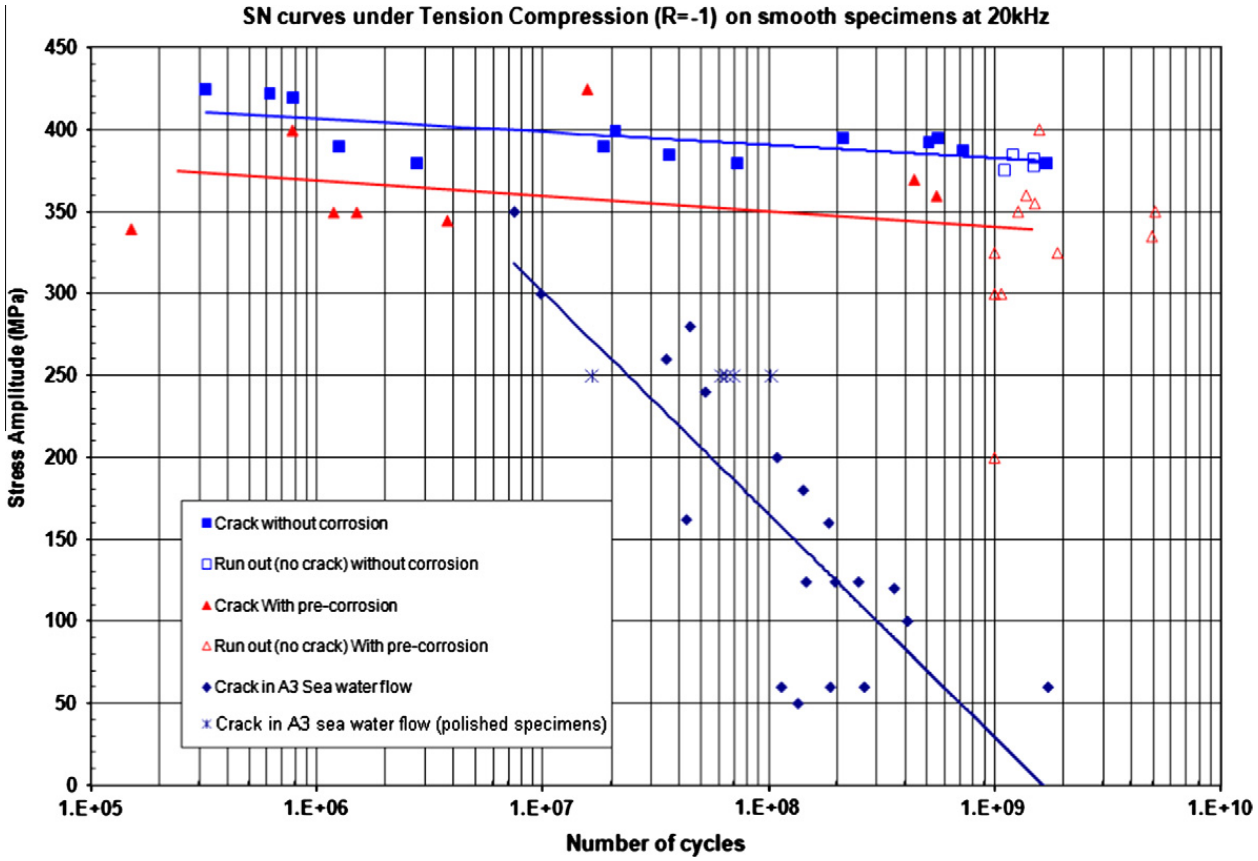

Fig. 5. S–N curves of the R5 steel under fully reversed tension at 20 kHz.

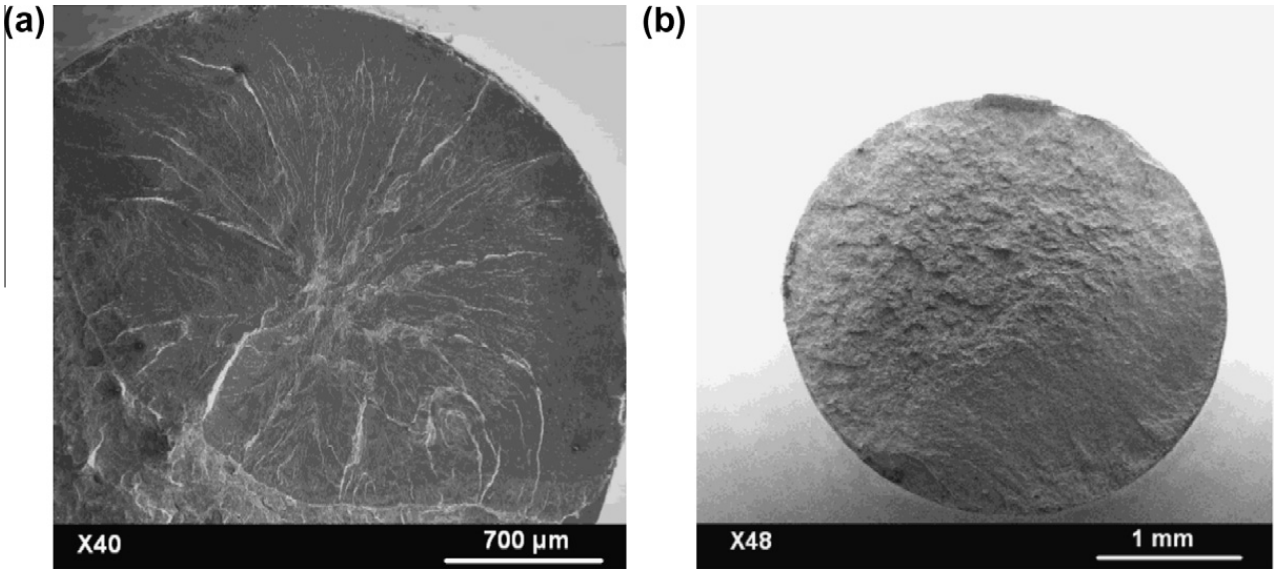

Fig. 6. Specimens without corrosion: (a) internal crack initiation $\sigma_a = 380$ MPa, $N_f = 2.78 \times 10^6$ cycles and (b) surface crack initiation $\sigma_a = 395$ MPa, $N_f = 5.61 \times 10^8$ cycles.

water flow the crack initiation areas were all around the specimen surface due to several large corrosion pits. The size of the pits depends on the time (that is to say the number of cycles). At the moment it is difficult to show undoubtful experimental evidence of the coupling between corrosion and the high strain rate due to the 20 kHz frequency. However the size of corrosion pits is larger under sea water flow (50–300 µm) than the pre-corroded specimens (30–80 µm). Furthermore, Fig. 8 right shows that all the flaws are perpendicular to the loading direction that is to say on the plane of maximum normal stress. This is probably characteristic of a corrosion/cyclic loading interaction. Finally, a specimen was tested under distilled

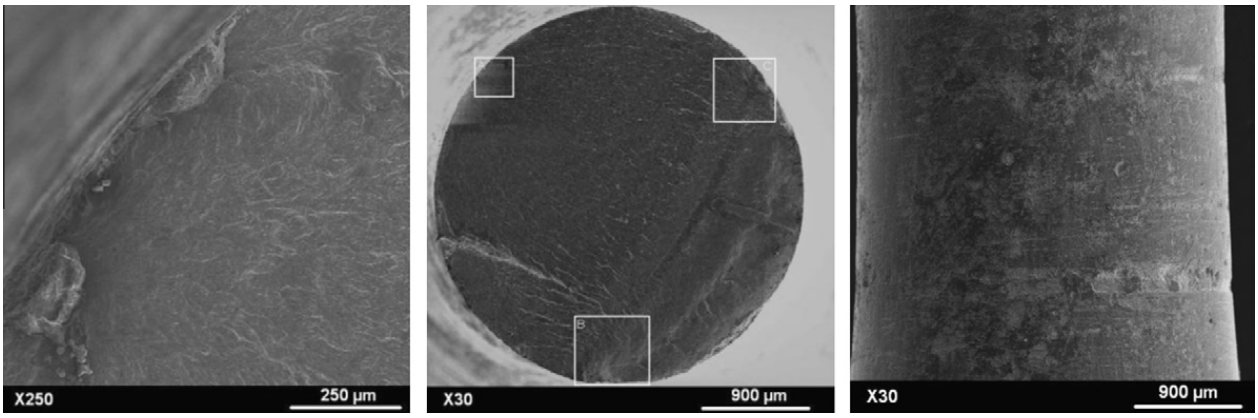

Fig. 7. Specimen with pre-corrosion, $\sigma_a = 370$ MPa, $N_f = 4.37 \times 10^8$ cycles.

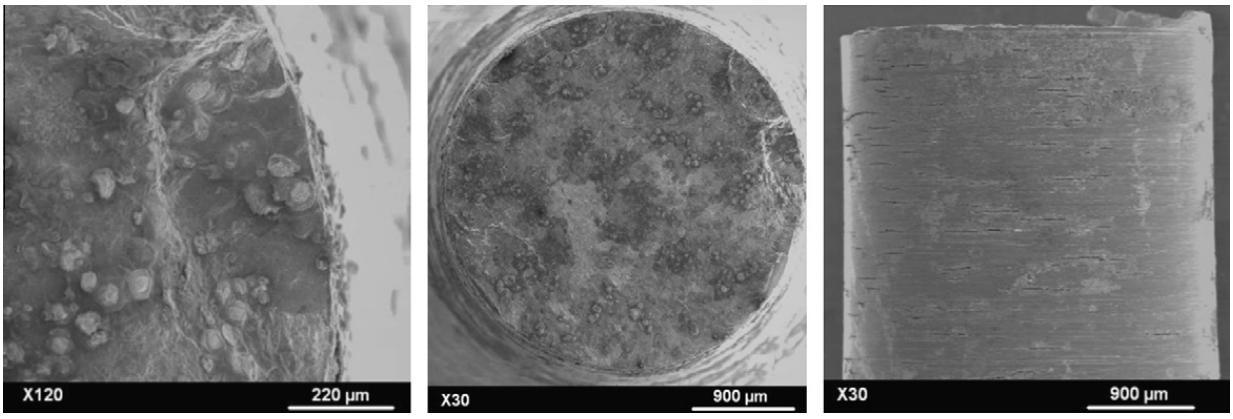

Fig. 8. Specimen tested under sea water flow, $\sigma_a = 160$ MPa, $N_f = 1.\ 8 \times 10^8$ cycles.

water flow (non-corrosive) under a stress amplitude of 200 MPa; no crack was observed after 10^9 cycles. This confirm a coupling between fatigue and corrosion.

Due to the high frequency of ultrasonic fatigue tests carried out in this study, the question of possible effects of the frequency on corrosion-fatigue strength in the gigacycle regime arises. Yeske and Roth [6] have shown that the corrosion-fatigue strengths of 403 stainless steel (a 12% Cr steel) exposed to concentrated chloride solution are the same at two very different loading frequencies: 40 Hz and 20 kHz. Although large effects were induced by environment change, the S–N curves in the range 10^7–10^8 cycles have a very good overlapping at the two frequencies. In this work [6], it is reported that cracks initiated at the base of the pits formed on the test specimens at both frequencies, even though some of the tests at 20 kHz lasted only a few 100 s.

A possible explanation for this similarity of the environmental effects at the two very different frequencies is proposed by Yeske and Roth. Transport of metal ions out of the pit electrolyte must occur at a high rate in ultrasonic fatigue but it appears that transport may be accelerated by convection induced by the high frequency loading. According to the authors of the present paper, further studies are needed to confirm this explanation and to really understand the physical mechanisms in corrosion-fatigue at high and relatively low frequency. The mechanisms are probably dependent on both the material properties and the corrosive environment. Anyway, ultrasonic fatigue tests in corrosive environment is the only reasonable fatigue tests which could provide experimental data for the very high cycle regime. With an industrial point of view, one has also to keep in mind that the artificial sea water A3 is much more corrosive than real sea water where R5 steel is used, another interesting point for industrial application is the roughness effect.

Some complementary fatigue tests were carried out under sea water flow at a stress amplitude of 250 MPa on some specimens with the same geometry but with a surface polished with emery paper ($Ra = 0.1$ µm). There was no evidence of the surface roughness effect under sea water flow: the fatigue life was the same than without polishing (Fig. 5). The poor corrosion-fatigue strength was related to the size of pits which are nearly hemispherical surface defects. Due to the major role of the defects, the proportion of the crack propagation period compared to the total life is studied in the following.

3.2.1. Assessment of the crack initiation and propagation duration

3.2.1.1. Fatigue crack growth results. Fatigue crack growth tests were carried out on three specimens. The $da/dN = f(\Delta K)$ curve is illustrated in Fig. 9. This shows that in air the mode I ($R = -1$) stress intensity threshold for R5 steel is around 3.3 MPa $m^{1/2}$.

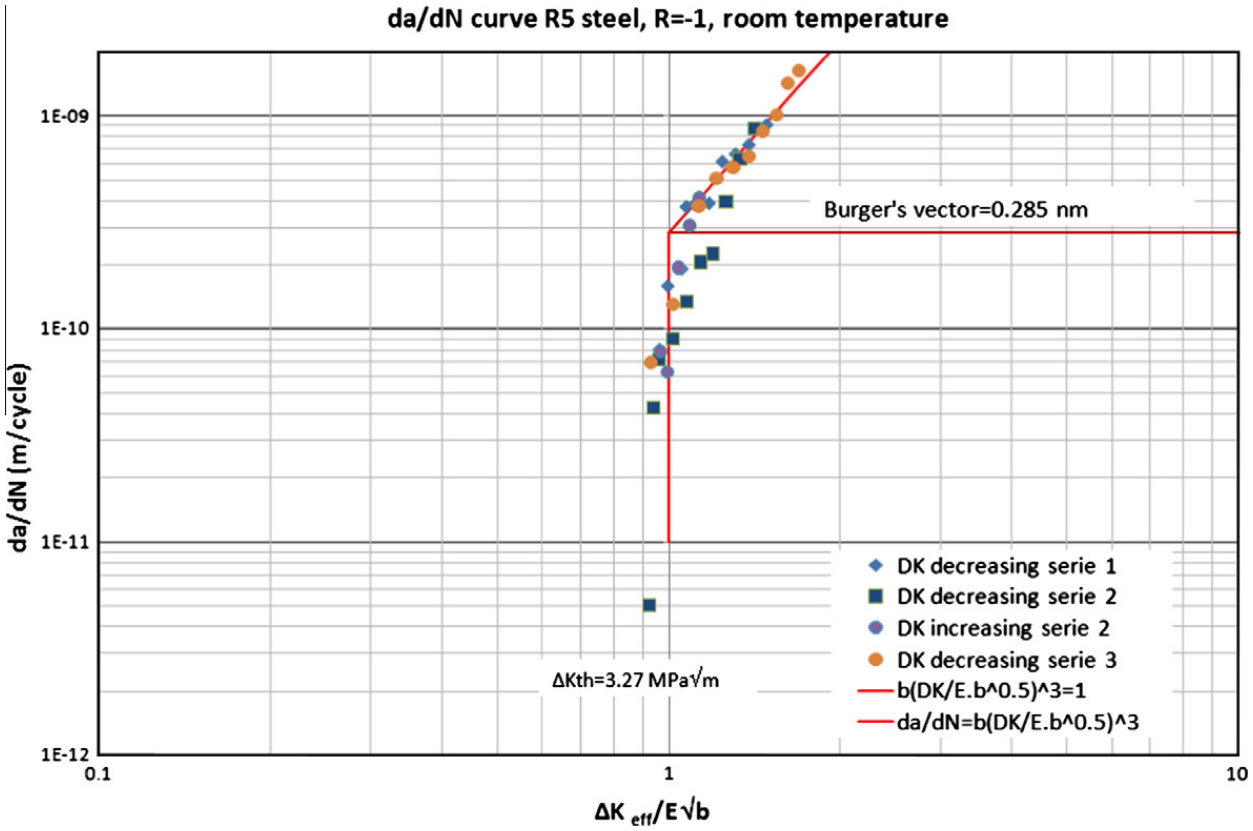

Fig. 9. Experimental crack growth curve at 20 kHz.

The fatigue crack propagation duration was estimated according to the work of Paris et al. [8,11], based on the Paris–Hertzberg–Mc Clintock crack growth rate $\frac{da}{dN} = b\left(\frac{\Delta K_{eff}}{E\sqrt{b}}\right)^3$ and $\left(\frac{\Delta K_{eff}}{E\sqrt{b}}\right) = 1$ at the corner, where E is the elastic modulus and b the Burger's vector of the material. Fig. 9 shows the agreement of this equation with our experimental data for E = 211 GPa and b = 0.285 nm. In our experiments at 20 kHz the measurement of K_{op} is not possible, thus in first approximation, $\Delta K_{eff} \sim K_{max}$ and no water interaction with the stress intensity factor was considered.

To assess the crack propagation phase, a corrosion pit was modelled by an hemispherical surface defect with radius R. A fatigue crack of depth a from the surface of the hemisphere and perpendicular to the loading direction was assumed due to inter-crystalline corrosion cracking. According to the asymptotic approximation proposed by Paris et al. [12] the crack tip stress intensity factor in mode I is: $K_I = \sigma\sqrt{\pi a}Y(x,\nu)$, where $x = a/R$, ν is the Poisson ratio and:

$$Y(x,\nu) = 1.015\left[A(\nu) + B(\nu)\left(\frac{x}{1+x}\right) + C(\nu)\left(\frac{x}{1+x}\right)^2 + D(\nu)\left(\frac{x}{1+x}\right)^3\right] \tag{2}$$

with: $A(\nu) = 1.683 + \frac{3.366}{7-5\nu}$, $B(\nu) = -1.025 - \frac{12.3}{7-5\nu}$, $C(\nu) = -1.089 + \frac{14.5}{7-5\nu}$, $D(\nu) = 1.068 - \frac{5.568}{7-5\nu}$.

It was assumed that the propagation of the fatigue crack is divided in three stages: (i) a short crack propagation during $N_{a_{int}-a_0}$ cycles, from initiation a_{int} to the crack size a_0, then (ii) a small crack propagation period of $N_{a_0-a_i}$ cycles, from a_0 to the crack size a_i, and (iii) a long crack propagation N_{a_i-a} cycles, from a_i to the final crack size a. In the short crack growth regime from a_{int} to the crack size a_0, it was assumed [8] that $\frac{da}{dN} = b\left(\frac{a}{a_0}\right)^{\alpha/2}$.

With these three different regimes (illustrated in Fig. 10) the very quick propagation of short crack and the quick propagation of small crack compared to long crack were considered. From [8] the three durations of the three previous stages are the following:

$$N_{a_{int}-a_0} = \frac{E^2}{Y_0^2\sigma_a^2\pi(\alpha/2-1)}\left[\left(\frac{a_0}{a_{int}}\right)^{(\alpha/2-1)} - 1\right] \tag{3}$$

$$N_{a_0-a_i} = \frac{2E^2}{Y_0^2\sigma_a^2\pi}\left[1 - \sqrt{\frac{a_0}{a_i}}\right], \text{ if it is assumed that } Y(a/R) \approx Y_0 = Y(a_0/R) \text{ from } a_0 \text{ to } a_i \tag{4}$$

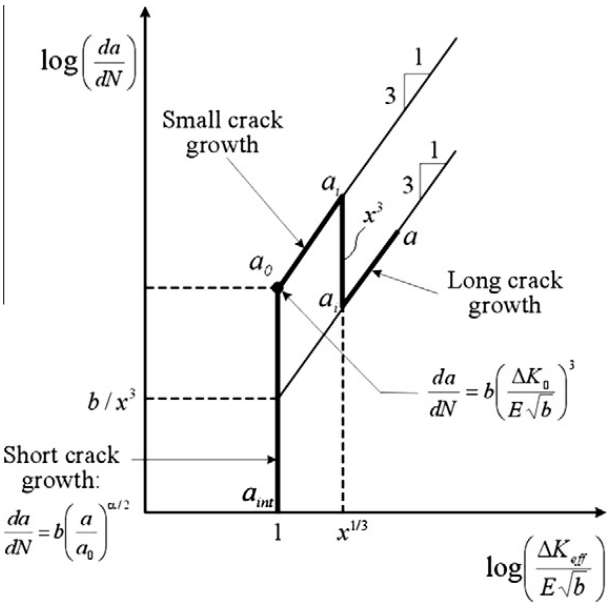

Fig. 10. Model of the fatigue growth behaviour for short, small and long cracks according to [11].

Table 3
Hemispherical surface crack growth vs. experimental fatigue life on some pre-corroded specimens with $x = 3$, $\alpha = 25$, 100 and 200, and different a_{int}/a_0 ratios.

α	a_{int}/a_0	$N_{a_{int}-a_0}$	$N_{a_0-a_i}$	N_{a_i-a}	N_{Prop} (cycles)	N_P (cycles)
Case 1: $\sigma_a = 360$ MPa, $R = 48$ μm, $a_0 = 9.32$ μm, $a = 2.4$ mm, $N_{experimental} = 5.5 \times 10^8$ cycles						
25	0.9	6704	44,151	4,507,080	4,557,935	539,600
	0.94	2947			4,554,178	
	0.97	1192			4,552,423	
100	0.9	115,801	44,151	4,507,080	4,667,032	
	0.94	13,163			4,564,394	
	0.97	2300			4,553,531	
200	0.9	11,184,860	44,151	4,507,080	15,736,091	
	0.94	150,676			4,701,907	
	0.97	6404			4,557,635	
Case 2: $\sigma_a = 370$ MPa, $R = 70$ μm, $a_0 = 7.104$ μm, $a = 2.15$ mm, $N_{experimental} = 4.4 \times 10^8$ cycles						
25	0.9	5113	23,220	1,402,860	1,431,193	510,836
	0.94	2248			1,428,328	
	0.97	909			1,426,989	
100	0.9	88,331	23,220	1,402,860	1,541,411	
	0.94	10,041			1,436,121	
	0.97	1754			1,427,834	
200	0.9	8,531,566	23,220	1,402,860	9,957,646	
	0.94	114,932			1,541,012	
	0.97	4884			1,430,964	
Case 3: $\sigma_a = 425$ MPa, $R = 37.5$ μm, $a_0 = 6.28$ μm, $a = 1.96$ mm, $N_{experimental} = 1.56 \times 10^7$ cycles						
25	0.9	4519	28,651	2,717,227	2,750,397	387,175
	0.94	1987			2,747,865	
	0.97	804			2,746,682	
100	0.9	78,065	28,651	2,717,227	2,823,943	
	0.94	8874			2,754,752	
	0.97	1550			2,747,428	
200	0.9	7,540,073	28,651	2,717,227	10,285,951	
	0.94	101,575			2,847,453	
	0.97	4317			2,750,195	

And with the assumption that $Y(a/R) \approx Y(a_i/R)$ from a_i to the final crack size a:

$$N_{a_i-a} = \frac{2E^2 Y_0}{Y(a_i/R)^3 \sigma_a^2 \pi}\left[x^3\sqrt{\frac{a_0}{a_i}} - x^3\sqrt{\frac{a_0}{a}}\right] \tag{5}$$

Table 4
Hemispherical surface crack growth vs. experimental fatigue life for some specimens under sea water flow with, $x = 3$, $\alpha = 25$, 100 and 200, and different a_{int}/a_0 ratios.

α	a_{int}/a_0	$N_{a_{int}-a_0}$	$N_{a_0-a_i}$	N_{a_i-a}	N_{Prop} (cycles)	N_P (cycles)
Case 4: $\sigma_a = 160$ MPa, $R = 300$ μm, $a_0 = 41.5$ μm, $a = 2.6$ mm, $N_{experimental} = 1.83 \times 10^8$ cycles						
25	0.9	29,840	168,014	10,258,700	10,456,554	2,731,700
	0.94	13,120			10,439,834	
	0.97	5306			10,432,020	
100	0.9	515,466	168,014	10,258,700	10,942,180	
	0.94	58,593			10,485,307	
	0.97	10,237			10,436,951	
200	0.9	49,787,104	168,014	10,258,700	60,213,818	
	0.94	670,703			11,097,417	
	0.97	28,504			10,455,218	
Case 5: $\sigma_a = 350$ MPa, $R = 200$ μm, $a_0 = 6.66$ μm, $a = 2.3$ mm, $N_{experimental} = 7.4 \times 10^6$ cycles						
25	0.9	4796	16,174	902,654	923,624	570,885
	0.94	2109			920,937	
	0.97	853			919,681	
100	0.9	82,854	16,174	902,654	1,001,682	
	0.94	9481			928,246	
	0.97	1645			920,473	
200	0.9	8,002,548	16,174	902,654	8,921,376	
	0.94	107,806			1,026,634	
	0.97	4582			923,410	
Case 6: $\sigma_a = 240$ MPa, $R = 220$ μm, $a_0 = 15.65$ μm, $a = 2.88$ mm, $N_{experimental} = 5.2 \times 10^7$ cycles						
25	0.9	11,267	44,271	2,431,480	2,487,018	1,214,122
	0.94	4954			2,480,705	
	0.97	2003			2,477,754	
100	0.9	194,621	44,271	2,431,480	2,670,372	
	0.94	22,123			2,497,874	
	0.97	3865			2,479,616	
200	0.9	18,797,746	44,271	2,431,480	21,273,497	
	0.94	253,232			2,728,983	
	0.97	10,762			2,486,513	
Case 7: $\sigma_a = 200$ MPa, $R = 290$ μm, $a_0 = 23.015$ μm, $a = 2.81$ mm, $N_{experimental} = 1.08 \times 10^8$ cycles						
25	0.9	16,566	67,524	3,624,895	3,708,984	1,748,336
	0.94	7283			3,699,701	
	0.97	2946			3,695,364	
100	0.9	286,158	67,524	3,624,895	3,978,576	
	0.94	32,528			3,724,946	
	0.97	5683			3,698,101	
200	0.9	27,639,000	67,524	3,624,895	31,331,418	
	0.94	372,337			4,064,755	
	0.97	15,824			3,708,242	

The effect of the two previous approximations: ($Y(a/R) \approx Y_0 = Y(a_0/R)$ and $Y(a/R) \approx Y(a_i/R)$) on the calculated number of cycles was checked by comparison with numerical integration of the crack growth curve. No significant effect was seen.

Finally, the total duration of the crack propagation is: $N_{Prop} = N_{a_{int}-a_0} + N_{a_0-a_i} + N_{a_i-a}$.The previous equations were applied to our data assuming that the initial crack has a length, a_0, corresponding to the corner: $\frac{da}{dN} = b; \frac{\Delta K_{eff}}{E\sqrt{b}} = 1$.

Some experimental cases were considered with $x = 3$, $\alpha = 25$, 100 and 200, and different a_{int}/a_0 ratios. For instance, in Table 3 a pre-corroded specimen with a pit of $R = 48$ μm with $N_{experimental} = 5.5 \times 10^8$ cycles. In Table 4 a pit with $R = 300$ μm for a specimen under sea water flow with a life of 1.83×10^8 cycles. In the first case 99.1% of the fatigue life is due to initiation. For the fifth case, 94% of the fatigue life was consumed by the initiation phase. One can notice that with a high α and large a_{int}/a_0 one obtains similar N_{Prop} results than with a low α and small a_{int}/a_0, that is because with a higher α the crack does not grow as far due to the slope of the da/dN curve in the threshold region, then a_{int}/a_0 must be larger, and with a lower α, a_{int}/a_0 must be smaller. Furthermore one can notice that an equally appropriate approximation of the crack growth period according to [8]: $N_P = \pi E^2/[2(\Delta\sigma)^2]$ gives results in the same order compared to N_{Prop} (it is a rough approximation).

Results and simulations in Table 3 show that the duration of the crack propagation period is small compared to the total life of the specimen except for $\alpha = 200$ and $a_{int}/a_0 = 0.9$. For the fatigue test under sea water flow the conclusion is the same: the fatigue life is dominated by the crack initiation regime as soon as the fatigue life is more than $\sim 10^7$ cycles.

Of course the previous calculations were carried out by assuming that the crack growth is the same in air and under sea water flow. Consequently some other investigations have to be done for assessing more precisely the crack growth curve under sea water flow. An additional point has to be kept in mind for the specimens tested under sea water flow: crack initiation may be simultaneous with corrosion pit growth, whereas this is not the case for pre-corroded specimens. In this paper the part of the fatigue crack trajectory respective to the corrosion pit growth has not been distinguished. This may lead to an error in the assessment of the duration of the crack growth period under sea water flow. But, since several authors have shown that the crack growth rate in humid air, or in water is an order of magnitude higher than in dry air, even if the corrosion pit growth would be considered with a model able to assess both the crack growth rate and the corrosion pit growth in a coupled model (the authors do not know such a model in literature), the duration of the crack propagation period should stay short compared to the total fatigue life.

4. Conclusion and prospects

Very high cycle fatigue tests were carried out up to 10^9 cycles on smooth specimens in hot rolled martensitic-bainitic steel under three different conditions: (i) virgin specimens, (ii) pre-corroded specimens and (iii) under artificial sea water flow during the fatigue test. The fatigue strength at 10^8 cycles is significantly reduced by a factor of 74% compared to the virgin specimens and of 71% compared to the pre-corroded ones. The assessment of the crack growth shows that crack initiation dominates the total fatigue life when $N > 10^7$ cycles. The proposed assessment is reasonable for pre-corroded specimens, but other studies must be done to study the effect of corrosion pits under real time sea water flow. The effect of sea water on the crack growth and the stress intensity factor also needs to be studied. A possible coupling between environment and high frequency cyclic loading should be studied too. However, ultrasonic fatigue test immersed in flowing sea water is the only experimental way to investigate very long life of steel under corrosion conditions.

Acknowledgements

The authors acknowledge Arts et Métiers ParisTech and Foundation Arts et Métiers for the financial support of P.C. Paris' stay at LAMEFIP. They acknowledge Vicinay Cadenas S.A. for its financial support, and both the PCP France-Mexique and the CONACYT for their financial support too.

References

[1] Bathias C, Paris PC. Gigacycle fatigue in mechanical practice. New York, USA: Marcel Dekker Publisher Co.; 2005.
[2] Marines I, Bin X, Bathias C. An understanding of very high cycle fatigue of metals. Int J Fatigue 2003;25:1101–7.
[3] Zuo JH, Wang Z, Han H. Effect of microstructure on ultra-high cycle fatigue behavior of Ti–6Al–4V. Mater Sci Engng A 2008;473:147–52.
[4] Ammar HR, Samuel AM, Samuel FH. Effect of casting imperfections on the fatigue life of 319-F and A356–T6 Al–Si casting alloys. Mater Sci Engng A 2008;473:65–75.
[5] Pang HT, Reed PAS. Microstructure effects on high temperature fatigue crack initiation and short crack growth in turbine disc nickel-base superalloy Udimet 720Li. Mater Sci Engng A 2007;448:67–9.
[6] Yeske RA, Roth LD. Environmental effects on fatigue of stainless steel at very high frequencies. In: Wells (Westinghouse) JM, Buck, Roth, Tien, editors. Ultrasonic fatigue. New York: The Metallurgical Society of AIME; 1982. p. 365–85.
[7] Ebara R, Yamada Y. Corrosion fatigue behaviour of 13Cr stainless steel and Ti–6Al–4V at ultrasonic frequency. In: Wells (Westinghouse) JM, Buck, Roth, Tien, editors. Ultrasonic fatigue. New York: The Metallurgical Society of AIME; 1982. p. 349–64.
[8] Paris PC. The relationship of effective stress intensity, elastic modulus and Burgers-vector on fatigue crack growth as associated with "fish eye" gigacycle fatigue phenomena. In: Proceedings of VHCF-3, Kyoto, Japan; September 2004. p. 1–13.
[9] Wu TY, Bathias C. Application of fracture mechanics concepts in ultrasonic fatigue. Engng Fract Mech 1994;47:683–90.
[10] Sun Z. Etude du seuil de fissuration à haute fréquence en fatigue et en fretting fatigue. Ph.D. Thesis. CNAM, Paris France; 2000.
[11] Marines I, Paris PC, Tada H, Bathias C. Fatigue crack growth from small to long cracks in VHCF with surface initiations. Int J Fatigue 2007;29:2072–8.
[12] Paris PC, Palin-Luc T, Tada H, Saintier N. Stresses and crack tip stress intensity factors around spherical and cylindrical voids and inclusions of differing elastic properties and with misfit sizes. In: Int conf crack paths, Vicenza, Italy; 23–25 September 2009. p. 485–502 [on CD Rom].